PHYSICAL REVIEW D **91,** 074505 (2015)

Dyon structures in the deconfinement phase of lattice gluodynamics: Topological clusters, holonomies, and Abelian monopoles

V. G. Bornyakov
Institute for High Energy Physics, 142281 Protvino, Russia;
Institute of Theoretical and Experimental Physics, 117259 Moscow, Russia;
and School of Biomedicine, Far Eastern Federal University, 690950 Vladivostok, Russia

E.-M. Ilgenfritz
Joint Institute for Nuclear Research, VBLHEP and BLTP, 141980 Dubna, Russia

B. V. Martemyanov
Institute of Theoretical and Experimental Physics, 117259 Moscow, Russia;
National Research Nuclear University MEPhI, 115409 Moscow, Russia;
and Moscow Institute of Physics and Technology, 141700 Dolgoprudny, Moscow Region, Russia

M. Müller-Preussker
Humboldt-Universität zu Berlin, Institut für Physik, 12489 Berlin, Germany
(Received 4 November 2014; published 6 April 2015)

The topological structure of lattice gluodynamics is studied at intermediate resolution scale in the deconfining phase with the help of a cluster analysis. UV-filtered topological charge densities are determined from a fixed number of low-lying eigenmodes of the overlap Dirac operator with three types of temporal boundary conditions applied to the valence quark fields. This method usually allows us to find all three distinguished (anti)dyon constituents in the gauge field of Kraan–van Baal–Lee–Lu (anti)caloron solutions. The clustering of the three topological charge densities in Monte Carlo generated configurations is then used to mark the positions of anticipated (anti)dyons of the corresponding type. In order to support this interpretation, inside these clusters, we search also for timelike Abelian monopole currents (defined in the maximally Abelian gauge) as well as for local holonomies with at least two approximately degenerated eigenvalues. Our results support the view that light dyon-antidyon pairs—in contrast to the heavy (anti)caloron dyon constituents—contribute dominantly to thermal Yang-Mills fields in the deconfinement phase.

DOI: 10.1103/PhysRevD.91.074505 PACS numbers: 11.15.Ha, 12.38.Aw, 12.38.Gc

I. INTRODUCTION

For lattice gauge theory, 1998 was a remarkable year, in particular for those interested in chirality and topology. The Ginsparg-Wilson [1] condition to be imposed on a Dirac operator and providing a solution of the chirality problem at finite lattice spacing was rediscovered [2], a concrete construction of the Neuberger overlap Dirac operator was proposed [3,4], and the relation to topological structure was clarified [2,5].

The paradigm of instantons as a semiclassical realization of topological structure at the infrared scale [6] found a competitor when P. van Baal and T. C. Kraan [7–9], and K.-M. Lee and C.-H. Lu [10], for the case of finite temperature, worked out a broader class of classical Euclidean solutions of Yang-Mills theory: calorons with arbitrary holonomy, called "KvBLL calorons" throughout this paper. These solutions have not reached the same level of acceptance and interest among lattice practitioners that instantons once had (see, for example, [11,12]). However, immediate response to the new solutions from the lattice community can be found in Refs. [13,14].

Three of us were among the authors of [15] who demonstrated first that cooling of confining lattice ensembles leads to the extraction of KvBLL multi-(anti)caloron solutions (see also [16]).

Shortly thereafter, D. Diakonov, who had been very active before trying to connect instantons with confinement, in particular by relating the instanton gas to monopole percolation [17,18], wrote his famous review *Instantons at Work* [19], to which he added, in a later version, the chapter, "Non-instanton semiclassical configurations." This extension has become the starting point of a new research direction. D. Diakonov, together with V. Petrov and other coworkers, calculated the analog of 't Hooft's instanton amplitude [20] and—following T. C. Kraan's work [21]—formalized the moduli space of calorons [22] in terms of dyon degrees of freedom.

A simulation of a random nontrivial holonomy caloron gas or liquid model already provided a much better behavior of the potential of a static quark-antiquark pair towards confinement [23] than the corresponding Harrington-Shepard caloron gas model (with trivial

holonomy) [24]. Surely influenced by Polyakov's work [25] on quark confinement by monopoles, D. Diakonov and V. Petrov then formulated a dyon (i.e. monopole) gas model of confinement [26], for which they have been able to present a closed analytical solution (for random monopole gas simulations, see [27,28]).

In fact, the idea to reformulate the statistical mechanics of a gas of multi-instantons in terms of the moduli space of their constituents ("instanton quarks") had already been discussed already much earlier for the two-dimensional nonlinear sigma model [29,30] by transforming the partition function into a Coulomb gas model of the constituents.

We are aware of recent papers by E. Shuryak and collaborators to formulate models dealing with the statistical mechanics of self-dual dyons (and anti-self-dual antidyons), partly including the effect of dynamical fermions [31,32]. We hope to come back to this problem. In our present context we want to refer to Ref. [33] dealing with the T dependence of the density of light and heavy (L and M) dyons in $SU(2)$ gluodynamics.

During our intensive search for evidence of calorons and dyons in Monte Carlo–generated lattice gauge field ensembles [15,34–38], we collaborated with P. van Baal [39,40].

In our recent work [41], after having searched for signatures for calorons and dyons for $SU(2)$ Yang-Mills theory by means of overlap modes [42–44], we have turned to pure $SU(3)$ lattice gauge theory. The aim was to find again hints for dyon structures (as topological clusters) very close to the deconfinement temperature, revealed by the topological charge density defined with the massless overlap Dirac operator. An infrared scale is introduced by restriction to a small number of modes of the overlap Dirac operator with low-lying eigenvalues ("fermionic filtering"), i.e. only zero modes and near-zero modes. In this analysis, three different types of boundary conditions have been applied. The motivation was that these clusters might eventually be viewed as dyons or antidyons, i.e. constituents of KvBLL calorons or anticalorons [8–10] which come in three varieties.

We have demonstrated how their abundance and the tendency either to recombine into calorons or to form pairs of different types depends on the temperature in the vicinity of the deconfinement phase transition at $T_d \simeq 300$ MeV. An increasing caloron dissociation has been observed when passing the transition towards temperature values slightly above T_d. Similar observations were reported earlier for the $SU(2)$ Yang-Mills case [42,44].

KvBLL (anti)calorons are (anti-)self-dual solutions of the classical $SU(3)$ Yang-Mills field equations with topological charge $Q_t = \pm 1$ and x_4 periodicity (the latter related to the inverse temperature). They are exhibiting characteristic features worth looking for in gauge field configurations provided by lattice simulations. In the case of the gauge group $SU(3)$, they consist of three constituents (monopoles or "dyons") into which calorons can dissolve under specific conditions, such that the dyon centers become separated sufficiently far away from each other. The constituents in this limit become "dyons" well separated and static in "time" x_4. Their integrated action values or "masses" are fully determined by the Polyakov loop at spatial infinity ("asymptotic holonomy"), while their locations can be identified as positions, where the local holonomy has at least two identical eigenvalues. Moreover, the zero mode as well as the low-lying eigenmodes of the massless Dirac operator become localized around only one of the constituents [45]—which constituent depends on the temporal boundary condition imposed on the Dirac operator defined in a finite space-time box. (See the Appendix in [41] which presents a brief summary of those aspects of caloron solutions essential also for our present study.)

Suppose for a moment that these objects, which are minimizing the Yang-Mills action, saturate the partition function in a semiclassical-like path-integral representation. One is tempted to assume that the ensemble-averaged Polyakov loop (as an order parameter for the deconfinement transition) determines their asymptotic holonomy and, therefore, in particular, also the mass ratio among the constituents of different types. Since for $T \gg T_d$ the spatially averaged Polyakov loop tends to one of the center values of $SU(3)$, one may expect that deeper in the deconfinement phase one type of the tentative dyon constituents becomes very heavy, while the others are light. Taking the statistical weight into account for the constituents of different types, the heavy constituents should be suppressed compared to the light ones. The calorons as joint objects become more and more suppressed, too, and we are left only with many light self-dual and anti-self-dual monopole constituents which negligibly contribute to the topological charge. This might explain why the topological susceptibility becomes suppressed at $T > T_d$ (in addition to the theoretically well-understood suppression of caloron sizes [20,46]), while an area law of spacelike Wilson loops is still observed. This picture, which emerged from our earlier $SU(2)$ lattice investigations [42,44], has not yet been confirmed for the more realistic case of $SU(3)$ gluodynamics at temperatures well above T_d.

In the lattice study of Ref. [41] we considered only T values very close to T_d, where the spatial average of the trace of the Polyakov loop was still fluctuating closely around the origin of the complex plane. In order to confirm the appearance of topological objects like KvBLL calorons and their dyon constituents, we studied the low-lying spectrum of the overlap Dirac operator together with the spatially local holonomy distribution. The latter required an appropriate, small number of (over-improved) cooling steps [47]. This cooling was found to shift the asymptotic holonomy towards the respective $SU(3)$ center values and also to influence the local holonomy inside topological clusters, which primarily have been determined by the

low-lying overlap eigenmodes [48] of the uncooled configurations. The consequence of this exercise was that the positions of approximate equality of two eigenvalues of the local holonomy became nicely correlated with the centers of topological clusters. This gave us confidence that what we are seeing at intermediate scales (of few lattice spacings) can be interpreted as (anti)caloron and (anti)dyon excitations as described by KvBLL solutions.

In the present paper, we are going a step further. First, we are going to a higher temperature $T \approx 1.5T_d$, and second, we employ another feature which becomes important in the deconfined phase: thermal monopoles on nearly static world lines [49–52]. Thermal monopoles are loops of magnetic currents wrapped around the x_4 direction. As we shall see, they are also characterizing dyon constituents by the occurrence of Abelian monopole world lines at their centers. Therefore, we transform our real lattice gauge field into the maximally Abelian gauge (MAG) and determine the corresponding magnetic currents after Abelian projection. In order to clarify the role of cooling for the Abelian monopole structure, we perform the gauge-fixing in two variants, without (before) and with (after) cooling (that we again apply as a few steps of over-improved cooling). We shall convince ourselves that the thermal monopoles are clearly correlated with the topological cluster centers determined from fermionic filtering. As a byproduct, it turns out that thermal monopoles are rather stable under (moderate) cooling, in contrast to the local holonomy.

In Sec. II we introduce our lattice setup, and in Sec. III we define the topologically relevant lattice observables employed later on. In Sec. IV, starting from analytic KvBLL caloron solutions, we construct (on a lattice) model gauge field configurations consisting of one heavy or two light dyon-antidyon pairs. We discuss how these pairs look from the following three points of view that we apply to analyze Monte Carlo generated thermal lattice gauge field configurations of $SU(3)$ gluodynamics: (i) from the topological cluster analysis based on the low-lying eigenmodes of the overlap operator, (ii) from the behavior of the local holonomy and its eigenvalues, and (iii) from the point of view of the MAG monopole current structure. Light dyon-antidyon pairs are supposedly the prototype of topological excitations in the bulk which guarantee the vanishing of the topological susceptibility. Moreover, we expect a dilute-gas admixture of rare and uncorrelated heavy (anti)dyon excitations. Our model configurations will easily allow us to distinguish between light and heavy dyon-antidyon pairs.

In Sec. V real gluodynamics is considered. The occurrence of a gap in the overlap eigenvalue spectrum depending on the fermionic boundary condition is demonstrated and compared to the reference cases of semi-analytical dyon-antidyon pairs. We construct the fermionic topological charge density with the help of a set of low-lying Dirac eigenmodes for all three different fermionic boundary conditions. Finally, the clusters of the three densities under consideration are presented, and their correlation to the local holonomy and to the static Abelian monopoles (obtained from the MAG construction) is analyzed.

As a result, we shall clearly identify a large fraction of light (anti)dyons and a smaller contribution of heavy (anti)dyons in the thermal lattice gluon fields in agreement with the qualitative picture of the deconfinement phase drawn above.

In Sec. VI we shall draw our main conclusions.

II. LATTICE SETUP

An ensemble of fifty $SU(3)$ gauge field configurations has been generated for this investigation by sampling the pure $SU(3)$ gauge theory on a lattice of size $20^3 \times 4$. We have used the Lüscher-Weisz action [53] with the value of the inverse coupling $\beta = 8.25$. In our previous work [41] we were using the same action at the same $\beta = 8.25$ but on a lattice of size $20^3 \times 6$. This choice was meant to describe configurations slightly above the deconfining temperature of $T_d \simeq 300$ MeV characteristic for pure $SU(3)$ gauge theory. This means that we are now addressing the deconfining phase at a temperature $T \simeq 1.5T_d$, while the lattice discretization scale is about $a \simeq 0.11$ fm.

Improved gauge actions are known to be mandatory for analyses using the overlap Dirac operator in order to take full advantage of the good chiral properties of the latter. For example, the sampled gauge fields are smoother than those sampled with the Wilson action. In particular, the idea of our analysis rests on the observation that changing the boundary condition leaves the number of zero modes unchanged if the field is smooth enough. The Lüscher-Weisz action has also been used in the QCDSF topological studies [54] of pure Yang-Mills theory with overlap fermions and by Gattringer and coworkers [55,56] when they were using a specific chirally improved fermion action for topological investigations. In the $SU(2)$ case, the tadpole-improved Symanzik action has been applied for analogous reasons in our previous work [42–44].

In addition to the plaquette term (pl), the Lüscher-Weisz action includes a sum over all 2×1 rectangles (rt) and a sum over all parallelograms (pg), i.e. all possible closed loops of length 6 along the edges of all 3-cubes

$$S[U] = \beta\Bigg(\sum_{pl}\frac{1}{3}\mathrm{ReTr}[1 - U_{pl}] + c_1\sum_{rt}\frac{1}{3}\mathrm{ReTr}[1 - U_{rt}] + c_2\sum_{pg}\frac{1}{3}\mathrm{ReTr}[1 - U_{pg}]\Bigg), \quad (1)$$

where the coefficients c_1 and c_2 are computed using results of one-loop perturbation theory and tadpole improvement [57–59]:

$$c_1 = -\frac{1}{20u_0^2}[1 + 0.4805\alpha], \qquad c_2 = -\frac{1}{u_0^2}0.03325\alpha. \tag{2}$$

For the given $\beta = 8.25$, the tadpole factor u_0 and the lattice coupling constant α have been self-consistently determined on a symmetric lattice (20^4) in a series of iterations via

$$u_0 = \left(\left\langle \frac{1}{3}\mathrm{ReTr}U_{pl}\right\rangle\right)^{1/4}, \qquad \alpha = -\frac{\ln(\langle\frac{1}{3}\mathrm{ReTr}U_{pl}\rangle)}{3.06839}, \tag{3}$$

arriving at the average plaquette value $\langle\frac{1}{3}\mathrm{ReTr}U_{pl}\rangle = 0.639172$.

III. TOPOLOGICALLY RELEVANT OBSERVABLES

The instruments (observables) of our analysis include (i) the local holonomy with its trace (i.e. the Polyakov loop), (ii) the (improved) gluonic topological charge, (iii) our definition of over-improved cooling, (iv) the Abelian monopoles revealed by Abelian projection in MAG, and (v) the fermionic topological charge density and its ultraviolet-filtered version, including the clustering properties of the latter.

In the context of topological structure, the meaning and usefulness of the finite-temperature holonomy (considered globally and locally to distinguish the dyonic constituents or "instanton quarks") has become recognized only through the discovery of the KvBLL-caloron solutions [8–10].

A. Holonomy

Let us begin with the local holonomy and its eigenvalues. The local holonomy is the product of timelike links

$$P(\vec{x}) = \prod_{x_0=1}^{N_\tau} U_0(\vec{x}, x_0) \tag{4}$$

having eigenvalues

$$\lambda_k = \exp(i2\pi\mu_k(\vec{x})), \tag{5}$$

which obviously depend on the spatial position.

On one hand, the spatial positions of the dyon constituents of KvBLL caloron solutions are determined by the condition that two of these eigenvalues should coincide (cf. Appendix in [41]). Later on we shall use this property to localize (anti)dyons in artificially modeled, as well as in simulated, lattice field configurations. On the other hand, the asymptotic holonomy of KvBLL calorons (after a suitable constant gauge transformation),

$$\mathcal{P}_\infty \equiv \lim_{|\vec{x}|\to\infty} P(\vec{x}) = \exp[2\pi i\,\mathrm{diag}(\mu_1, \mu_2, \mu_3)], \tag{6}$$

with real and ordered numbers $\mu_1 \le \ldots \le \mu_3 \le \mu_4 \equiv 1 + \mu_1$ and $\mu_1 + \mu_2 + \mu_3 = 0$) determines the masses of well-separated dyon constituents via $8\pi^2\nu_m$, where $\nu_m \equiv \mu_{m+1} - \mu_m$ (cf. Appendix in [41]).

Taking the trace of $P(\vec{x})$ one gets the (gauge invariant) complex-valued Polyakov loop

$$L(\vec{x}) = \frac{1}{3}\mathrm{Tr}P(\vec{x}). \tag{7}$$

For $SU(3)$, the condition of two coinciding eigenvalues of the local holonomy corresponds to the respective Polyakov loop being located on the periphery of the Polyakov triangle. All three eigenvalues coincide only in its corners with $L(\vec{x}) = z_k = \exp(ik2\pi/3)\cdot\mathbf{1}$ with $k = 0, 1, 2$. We call $\bar{L}$ the spatially averaged Polyakov loop of a given gauge field configuration:

$$\bar{L} = \frac{1}{V}\sum_{\vec{x}} L(\vec{x}). \tag{8}$$

Averaged appropriately over the statistical ensemble of gauge fields, it serves as an order parameter for the deconfinement transition of pure Yang-Mills theory. The latter has a global $Z(3)$ symmetry of the action, and the deconfined phase is characterized by the spontaneous breaking of this symmetry; i.e., the nonvanishing spatially averaged Polyakov loop, falling into one of the three sectors, can be represented as $\bar{L} \approx |\bar{L}|z_k$. For finite systems, transitions between the $Z(3)$ sectors (i.e. between different deconfined phases) are not excluded. Therefore, we consider all configurations with nonvanishing $\bar{L}$ transformed by a $Z(3)$ flip to the real sector where $\bar{L} \approx |\bar{L}|z_0$.

At this point it is probably worth underlining that the local holonomies we search for in the following will be related to the positions of the (anti)dyons in clusters of topological charge and not to their closeness to the center values of $SU(3)$ as was the aim in Ref. [60].

B. The gluonic definition of the topological density

The continuum definition of topological charge density is

$$q(x) = \frac{1}{16\pi^2}\mathrm{Tr}(F_{\mu\nu}(x)\tilde{F}_{\mu\nu}(x)) \tag{9}$$

with

$$\tilde{F}_{\mu\nu}(x) = \frac{1}{2}\epsilon_{\mu\nu\lambda\sigma}F_{\lambda\sigma}(x). \tag{10}$$

The (improved) gluonic topological charge density on the lattice rests on the field strength definition of $F^{(n)}_{\mu\nu}(x)$ as a "clover" average over all untraced plaquette loops (with sidelength $n = 1$) and over four untraced extended quadratic loops of size $n \times n$ (with $n = 2, 3$ in the improved case) within the $\mu\nu$ plane, placed around each site x and kept

untraced in that site x [61]. The improved topological charge and the corresponding continuum action (in units of the one-instanton action $S_{\rm inst}$) are then defined as

$$Q_{\rm glue} = \sum_x q(x), \tag{11}$$

$$S/S_{\rm inst} = \sum_x {\rm Tr}(F_{\mu\nu}(x)F_{\mu\nu}(x))/(16\pi^2). \tag{12}$$

C. Cooling and over-improved cooling

Cooling is an *ad hoc* method to remove quantum fluctuations up to a certain "diffusion" scale from given lattice field configurations created in the course of Monte Carlo simulations. It proceeds by a sweep over the lattice links, where the link is updated in such a way to warrant the minimum of action relative only to this link $U_{x,\mu} \in SU(3)$, while all other links remain untouched. For the $SU(3)$ gauge group, this local minimization is realized in the form of a sweep over three $SU(2)$ subgroups of $SU(3)$ (Cabibbo-Marinari method). Cooling can be defined with respect to different gluonic actions, not necessarily the action used for the Monte Carlo generation of the ensemble to work on. The simplest case is with respect to the Wilson (one-plaquette) action. More generally, cooling is defined with respect to an action of the form

$$S(\epsilon) = \sum_{x,\mu\nu} \frac{4-\epsilon}{3} {\rm ReTr}(1 - U_{x,\mu\nu}) + \sum_{x,\mu\nu} \frac{1-\epsilon}{48} {\rm ReTr}(1 - U^{2\times 2}_{x,\mu\nu}), \tag{13}$$

which reduces to Wilson action in the case $\epsilon = 1$. The so-called over-improved action [47] corresponds to $\epsilon = -1$. Expanding in powers of lattice spacing a, one finds

$$S(\epsilon) = \sum_{x,\mu\nu} a^4 {\rm Tr}\left[\frac{1}{2}F^2_{\mu\nu}(x) - \frac{\epsilon a^2}{12}(D_\mu F_{\mu\nu}(x))^2\right] + O(a^8). \tag{14}$$

For a discretized continuum instanton of size ρ, this provides

$$S(\epsilon) = 8\pi^2\left[1 - \frac{\epsilon}{5}\left(\frac{a}{\rho}\right)^2 + \mathcal{O}\left(\left[\frac{a}{\rho}\right]^4\right)\right], \tag{15}$$

suggesting that ρ under cooling will decrease for $\epsilon > 0$ and increase for $\epsilon < 0$. The inversion of lattice artifacts relative to the Wilson case makes topological lumps stable against cooling.

It is worth noting that standard cooling ($\epsilon = 1$)—averaged over gauge field ensembles—can be nicely mapped one to one [62] to the theoretically well-understood Wilson or gradient flow [63–65]. We believe the same to hold for over-improved cooling.

D. The overlap Dirac operator, the near-zero band and the UV filtered topological density

The next of our tools is the construction of the near-zero-mode band of eigenmodes of the massless overlap operator D. The overlap Dirac operator D fulfills the Ginsparg-Wilson equation [1]. A possible solution—for any *input Dirac operator*, in our case for the Wilson-Dirac operator D_W—is the following zero-mass overlap Dirac operator [3,4],

$$D(m=0) = \frac{\rho}{a}\left(1 + \frac{D_W}{\sqrt{D_W^\dagger D_W}}\right) = \frac{\rho}{a}(1 + {\rm sgn}(D_W)), \tag{16}$$

with $D_W = M - \frac{\rho}{a}$, where M is the hopping term of the Wilson-Dirac operator and $\frac{\rho}{a}$ a negative mass term usually subject to optimization. The index of D, i.e. the difference in its number of right-handed and left-handed zero modes, can be identified with the integer-valued topological charge $Q_{\rm over}$ [5].

The topological charge density with maximal resolution (down to the lattice spacing a) is defined in terms of the overlap Dirac operator as follows,

$$q(x) = -{\rm tr}\left[\gamma_5\left(1 - \frac{a}{2}D(m=0;x,x)\right)\right]. \tag{17}$$

Using the spectral representation of (17) after diagonalization (using a variant of the Arnoldi algorithm) in terms of the eigenmodes $\psi_j(x)$ with eigenvalue λ_j, a UV smoothed form of the density can be defined by filtering, i.e. summing over a narrow band of near-zero eigenmodes,

$$q_N(x) = -\sum_{j=1}^{N}\left(1 - \frac{\lambda_j}{2}\right)\sum_c (\psi^c_j(x), \gamma_5\psi^c_j(x)), \tag{18}$$

summed over color c and with λ_N as a UV cutoff.

While the physical fermion sea is described by a Dirac operator with antiperiodic boundary condition, for the analysis of topological structure it is useful to diagonalize the overlap Dirac operator with a continuously modified boundary condition, which is characterized by an angle ϕ,

$$\psi(\vec{x}, x_4 + \beta) = \exp(i\phi)\psi(\vec{x}, x_4). \tag{19}$$

We have chosen three angles,

$$\phi = \left\{ \begin{array}{l} \phi_1 \equiv -\pi/3 \\ \phi_2 \equiv +\pi/3 \\ \phi_3 \equiv \pi \end{array} \right\}, \tag{20}$$

ensuring for a single caloron solution that the corresponding fermion zero modes become maximally localized at each, but always at one of its three constituent dyons. Note that ϕ_3 corresponds to the antiperiodic boundary condition. Only the spectrum corresponding to the latter boundary condition (no matter whether the gauge field ensemble is quenched or not) develops a gap in the high-temperature phase (see Ref. [66]).

On the contrary, for the confined phase of gluodynamics (as well as for the chirally broken phase of QCD), it is known that the gross features of the Dirac spectrum are only weakly dependent on the boundary conditions.

In the deconfined (high-temperature) phase, the construction of the UV smoothed topological charge density in terms of the eigenvalues and eigenmodes should be specifically done for the three boundary conditions,

$$q_{i,N}(x) = -\sum_{j=1}^{N}\left(1-\frac{\lambda_{i,j}}{2}\right)\sum_{c}(\psi^{c}_{i,j}(x),\gamma_5\psi^{c}_{i,j}(x)), \quad (21)$$

where $i = 1, 2, 3$ enumerates the three boundary conditions defined by Eq. (20) and j enumerates the eigenvalues $\lambda_{i,j}$ arranged in increasing order $\lambda_{i,1} < \lambda_{i,2} < \ldots < \lambda_{i,N}$.

Let us note here that topologically nontrivial clusters filtered out with the truncated densities (21) and averaged over the boundary conditions can be nicely mapped onto the ones seen with the gluonic definition (9) after an optimized number of APE or STOUT smearing steps [67–69]. We have no doubt that this will hold also when applying the Wilson flow accordingly [63–65].

E. MAG and Abelian monopoles definitions

We use the definition of MAG introduced for lattice $SU(N)$ theory in [70] and later specified for the $SU(3)$ group in [71]. The MAG is fixed by maximizing the functional,

$$F[U] = \frac{1}{12V}\sum_{x,\mu}[|(U_\mu(x))_{11}|^2 + |(U_\mu(x))_{22}|^2 + |(U_\mu(x))_{33}|^2], \quad (22)$$

with respect to local gauge transformations g of the lattice gauge field,

$$U_\mu(x) \to U^g_\mu(x) = g(x)^\dagger U_\mu(x) g(x+\hat{\mu}). \quad (23)$$

Note that alternative definitions of the MAG for the $SU(3)$ group were introduced in [72] and were recently studied in [73]. We use the simulated annealing algorithm first used to fix MAG in the $SU(2)$ case [74] and then extended to the $SU(3)$ group in [75]. The details of the implementation of simulated annealing for the case of the $SU(3)$ gauge group can be found in [76]. To reduce the effects of ambiguities due to Gribov copies, we have always generated ten random gauge copies and have picked up the copy with the maximal value of the gauge fixing functional.

The Abelian field $u_\mu(x) \in U(1)\times U(1)$ is determined as

$$u_\mu(x) = \mathrm{diag}(u^{(1)}_\mu(x), u^{(2)}_\mu(x), u^{(3)}_\mu(x)), \quad (24)$$

where

$$u^{(a)}_\mu(x) = e^{i\theta^{(a)}_\mu(x)}, \quad (25)$$

with

$$\theta^{(a)}_\mu(x) = \arg(U_\mu(x))_{aa} - \frac{1}{3}\sum_{b=1}^{3}\arg(U_\mu(x))_{bb}|_{\mathrm{mod}2\pi}, \quad (26)$$

such that

$$\theta^{(a)}_\mu(x) \in \left[-\frac{4}{3}\pi, \frac{4}{3}\pi\right]. \quad (27)$$

This definition of Abelian projection $u_\mu(x)$ maximizes the expression $|\mathrm{Tr}(U^\dagger_\mu(x)u_\mu(x))|^2$ [77].

The monopole currents are residing on links of the dual lattice and are defined by

$$j^{(a)}_\mu(^*x) = \frac{1}{2\pi}\epsilon_{\mu\nu\alpha\beta}\partial_\nu\bar{\theta}^a_{\alpha\beta}(x) = 0, \pm 1, \pm 2, \quad (28)$$

where ∂_ν is the forward lattice derivative, and the Abelian flux $\bar{\theta}^a_{\mu\nu} \in (-\pi, \pi]$ is defined from the Abelian plaquette,

$$\theta^{(a)}_{\mu\nu}(x) = \partial_\mu\theta^{(a)}_\nu(x) - \partial_\nu\theta^{(a)}_\mu(x), \quad (29)$$

using the relation

$$\theta^{(a)}_{\mu\nu}(x) = \bar{\theta}^{(a)}_{\mu\nu}(x) + 2\pi m^a_{\mu\nu}(x). \quad (30)$$

They are then shifted by $2\pi n$ to satisfy

$$\sum_{a=1}^{3}\bar{\theta}^{(a)}_{\mu\nu}(x) = 0. \quad (31)$$

This guarantees that

$$\sum_{a=1}^{3} j^{(a)}_\mu(x) = 0; \quad (32)$$

i.e., only two currents are independent. The current conservation law is satisfied for every a separately:

$$\sum_{\mu}\partial^-_\mu j^{(a)}_\mu(s) = 0, \qquad a = 1, 2, 3. \quad (33)$$

IV. CONSTRUCTING (ANTI)DYON PAIRS

The analytic construction of an $SU(3)$ caloron is described in Ref. [8]. It can be used in order to create model configurations of the type we might expect to be dominant in the thermalized gauge field configurations at $T = 1.5T_d$ studied in this paper. Therefore, we have chosen model calorons with an asymptotic holonomy $\mathcal{P}_\infty = \exp[2\pi i \mathrm{diag}(\mu_1, \mu_2, \mu_3)]$ with $\mu_1 = -\mu_3 = -0.271$ and $\mu_2 = 0$ such that its Polyakov loop value is $L = \frac{1}{3}\mathrm{Tr}\mathcal{P}_\infty = (2\cos(2\pi\mu_1) + 1)/3 = 0.24$. This value corresponds to the averaged Polyakov loop $\langle|\bar{L}|\rangle$ observed for the thermalized gauge field configurations at $1.5T_d$.

Modeling gauge field ensembles with calorons and their constituents in this way should include a self-consistent (bootstraplike) determination of the average Polyakov loop to be equal to the trace of the asymptotic holonomy of the superposed semiclassical objects, which also includes a fine-tuning of the properties of the different types of dyons. We refer to [23], where this strategy in the case of the gauge group $SU(2)$ for varying temperature has been approximately realized with a random gas of calorons and anticalorons. This modeling was triggered by our understanding of the confinement phase, where the Polyakov loop fluctuates around zero. Within the maximally nontrivial-holonomy $SU(2)$ caloron, the Polyakov loop varies from zero (i.e. the asymptotic value) inside the constituents to $+1$ and -1, respectively, which provides an almost zero Polyakov loop average even for a single caloron.

In our present $SU(3)$ case, two of the three constituent dyons are light (i.e. if well separated they carry the topological charge fraction $\nu_1 = \nu_2 = 0.271$) and the third becomes heavier ($\nu_3 = 0.458$). The local Polyakov loops at the dyon positions happen to be located on the sides of the Polyakov triangle as pointed out in Pierre van Baal's review [78] and in the Appendix of Ref. [41].

In order to construct a dyon-antidyon pair of the third (heavy) type, we have placed the dyon-triplet of such a caloron solution at positions

$$\begin{aligned} x_1 &= -1, \quad y_1 = -10, \quad z_1 = 0 \\ x_2 &= 1, \quad y_2 = -10, \quad z_2 = 0 \\ x_3 &= 0, \quad y_3 = 1, \quad z_3 = 0 \end{aligned} \tag{34}$$

with the local Polyakov loop values,

$$\begin{aligned} L(\vec{x}_1) &= L(\vec{x}_2)^* = 0.395 - i * 0.171, \\ L(\vec{x}_3) &= -0.333, \end{aligned}$$

and calculated the potentials for $-2.5 < x, z < 2.5$ in the positive-y half-space $0 < y < 2.5$ (all numbers are given in units of the time period of periodic caloron solution). Note that the light dyons are far outside the region where the gauge field is calculated. Similarly, we have placed antidyons (as constituents of a corresponding anticaloron solution) at

$$\begin{aligned} \bar{x}_1 &= -1, \quad \bar{y}_1 = 10, \quad \bar{z}_1 = 0 \\ \bar{x}_2 &= 1, \quad \bar{y}_2 = 10, \quad \bar{z}_2 = 0 \\ \bar{x}_3 &= 0, \quad \bar{y}_3 = -1, \quad \bar{z}_3 = 0 \end{aligned} \tag{35}$$

and calculated their potentials for $-2.5 < x, z < 2.5$ in the negative-y half-space $-2.5 < y < 0$. Finally, we have sewed together these potentials defined in their respective domains and—for the purpose of discretization—have calculated links on a $20 \times 20 \times 20 \times 4$ lattice (with lattice spacing equal to $1/4$). This lattice covers the full spatial region $-2.5 < x, y, z < 2.5$ and the temporal periodicity range $0 < t < 1$. On this lattice the dyon is at position (10, 14, 10) and the antidyon at (10, 6, 10). Next, cooling has been applied to the constructed lattice field configuration in order to remove the discontinuites left over from sewing together the half-spaces and in order to arrange for smooth spatially periodic boundary conditions (spatial torus).

We have analyzed the obtained configuration by diagonalizing the overlap Dirac operator and identifying $N = 20$ near-zero eigenvalues and respective eigenmodes. The diagonalization has been performed for three temporal boundary conditions (20). The pattern of near-zero eigenvalues of the overlap operator is shown in Fig. 1 for the three types of boundary conditions. Note that the spectrum develops a gap for the first and second kind of boundary conditions, while there are near-zero eigenvalues for the third kind.

The profile of the gluonic topological charge density (as described in Sec. III B) over the xy plane that contains the dyon-antidyon pair is shown in Fig. 2(a). In the same plane, static MAG thermal monopoles are found. Their positions are visualized in Fig. 2(b). Here and in the following we will have only temporal ($\mu = 4$) magnetic currents $j_4^{(a)}(x)$, and these are of three types: $(\pm 1, \mp 1, 0)$, $(0, \pm 1, \mp 1)$, $(\mp 1, 0, \pm 1)$, which will form closed loops in the temporal direction.

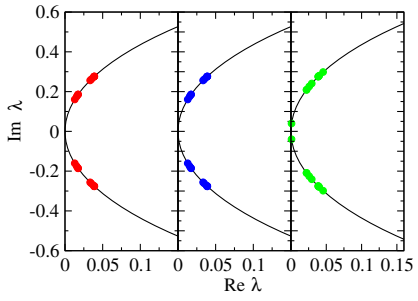

FIG. 1 (color online). Overlap eigenvalues for a heavy (third-type) dyon-antidyon pair for the three different boundary conditions of Eq. (20).

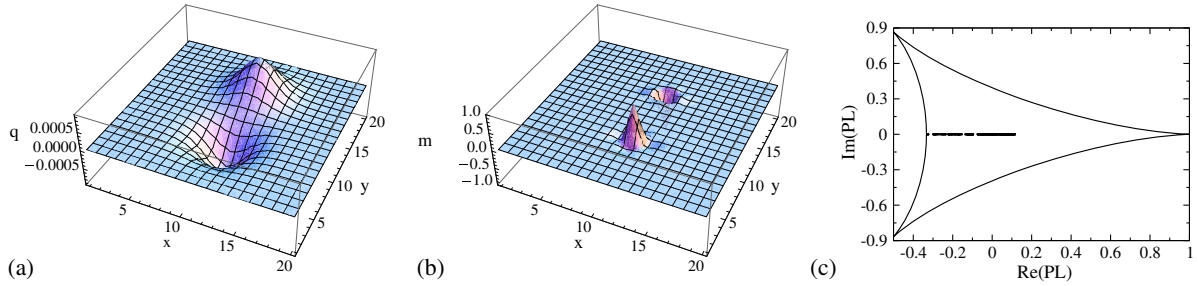

FIG. 2 (color online). A heavy (third-type) dyon-antidyon pair is presented (a) by the profile of gluonic topological charge density over the xy plane, (b) by the local magnetic charge distribution of (static, timelike) MAG monopole currents in the xy plane, and (c) a scatter plot of the Polyakov loop values taken at the same plane.

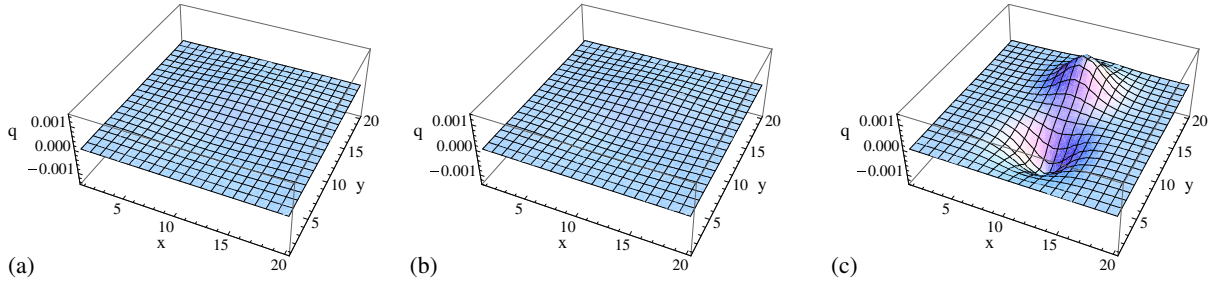

FIG. 3 (color online). The fermionic topological charge densities (a), (b), (c) are shown for the heavy dyon-antidyon pair reconstructed from the eigenmodes, corresponding to the three types of boundary conditions.

For the given configuration, the same xy plane is mapped to the complex plane of the Polyakov loop. The scatter plot Fig. 2(c) shows the local Polyakov loop of the isolated heavy dyon-antidyon pair as the part of the real axis connecting the origin with the left side of the Polyakov triangle.

Using $N = 20$ low-lying eigenmodes of the overlap Dirac operator, we have reconstructed the profiles of the fermionic topological charge density according to the spectral representation of the latter (21) for the three temporal boundary conditions (20). Only the third boundary condition catches the topological charge profile of the dyon-antidyon pair of the third (heavy) type (see Fig. 3).

This example of a dyon-antidyon pair demonstrates that there is a strong correlation between clusters of gluonic as well as fermionic topological charge density on the one hand and MAG monopoles on the other.

Another example of an artificial dyon-antidyon system is a pair of two light dyon-antidyon pairs formed out of the two light types (first and second) of the same caloron solution as discussed above. For this purpose we have placed the constituents of the caloron at

$$\begin{aligned} x_1 &= -1, \qquad y_1 = 1, \qquad z_1 = 0 \\ x_2 &= 1, \qquad y_2 = 1, \qquad z_2 = 0 \\ x_3 &= 0, \qquad y_3 = -10, \qquad z_3 = 0 \end{aligned} \tag{36}$$

and those of the corresponding anticaloron at

$$\begin{aligned} \bar{x}_1 &= -1, \qquad \bar{y}_1 = -1, \qquad \bar{z}_1 = 0 \\ \bar{x}_2 &= 1, \qquad \bar{y}_2 = -1, \qquad \bar{z}_2 = 0 \\ \bar{x}_3 &= 0, \qquad \bar{y}_3 = 10, \qquad \bar{z}_3 = 0, \end{aligned} \tag{37}$$

respectively, and applied the same cut-and-paste procedure for the half spaces $y > 0$ and $y < 0$ as before.

The pattern of near-zero eigenvalues of the overlap operator for the extracted light double-dyon–antidyon pair is shown in Fig. 4 for the three types of boundary conditions. Now we observe a clear gap opening around zero for the third kind of boundary condition, while for the other ones near-zero eigenvalues occur.

The gluonic topological charge density, as well as the set of monopole currents, shows all dyons and antidyons,

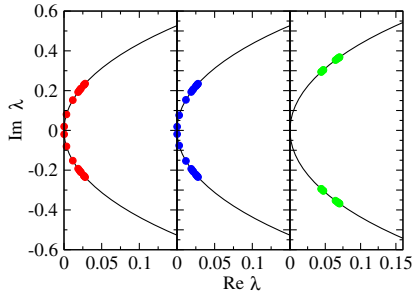

FIG. 4 (color online). Overlap eigenvalues for a light double-dyon–antidyon pair for the three different boundary conditions of Eq. (20).

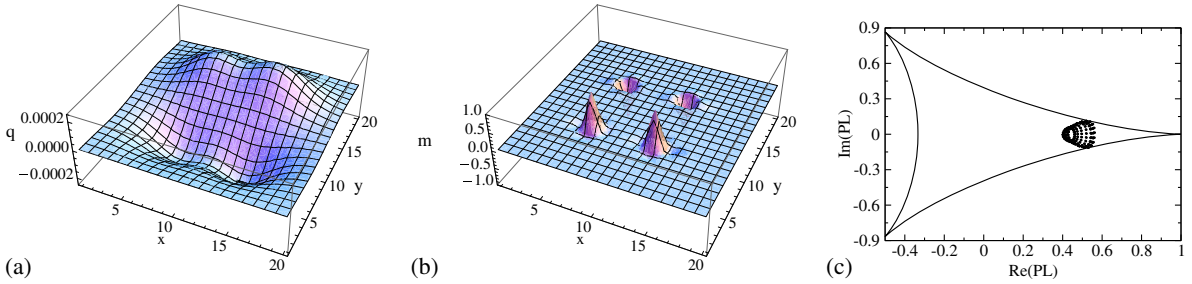

FIG. 5 (color online). For the light double-dyon–antidyon pair we show (a) the profile of gluonic topological charge density on the xy plane, (b) the local magnetic charge distribution of (static, timelike) MAG monopole currents in the xy plane and (c) a scatter plot of the Polyakov loop values picked up at the same plane.

independent of their type, as can be seen in Fig. 5(a) and Fig. 5(b). The Polyakov loop scatter plot for the (light) double-dyon–antidyon pair [cf. Fig. 5(c)] is not a simple combination of Polyakov loop plots for single dyon-antidyon pairs of a given type [compare with Fig. 2(c)], but has a dispersed form due to the influence of dyons (antidyons) of different type on each other.

For the same configuration the fermionic topological charge densities are shown in Fig. 6. As expected, only the first and second type of fermionic boundary conditions visualizes topological lumps; more precisely, each of them visualizes the respective pair of a light dyon and antidyon.

Let us finally mention that an alternative approach to studying dyon-antidyon pairs has been chosen very recently in [79] by putting a hedgehog ansatz of (anti)dyon solutions on a lattice and investigating its behavior under gradient flow.

V. RESULTS FOR THE YANG-MILLS ENSEMBLE

In the following we will analyze the gluodynamics ensemble of 50 thermalized configurations along the lines sketched above for the model dyon-antidyon pairs. For identifying topological clusters of the lattice gauge fields with the help of the low-lying spectrum of the overlap operator, we used a fixed number of 20 lowest modes always determined before any cooling or smearing was applied. In order to detect gluonic features of (anti)dyon excitations inside such clusters, we employed four steps of over-improved cooling [47]. This amount of cooling changes (clarifies) the conformation of what we call the thermal monopole structure. The number of thermal monopoles was reduced by an approximate factor 2, and they became strictly static. Cooling beyond that stage kept the monopole number stable for a long period of cooling. Within four cooling steps, we did not completely match the topological profiles (gluonic and fermionic) as we did in our previous paper [41] where we followed the concept of an equivalent filtering as developed in [67–69].

In Fig. 7(a) we show a scatter plot of the spatially averaged Polyakov loop $\bar{L}$ obtained from the ensemble of 50 generated configurations. The (black) points concentrated around $\bar{L} \simeq 0.24$ belong to the Monte Carlo equilibrium configurations, while the shifted (red) points (around $\bar{L} \simeq 0.75$) correspond to the same configurations but after the four steps of over-improved cooling.

It is clearly seen that the $Z(3)$ symmetry is spontaneously broken for the equilibrium configurations as expected for temperatures above the critical one. (Over-improved) cooling enhances this effect. Identifying the average $\langle \bar{L} \rangle \simeq 0.24$ with the asymptotic holonomy of an assumed dyon-antidyonic content of the gauge fields, we conclude that such content would render dyons of the first and second type lighter than dyons of the third type. Therefore, we expect for equilibrium configurations that dyons of the third (heavy) type will gain a smaller statistical weight. (This differs from the situation of maximally nontrivial holonomy in the confinement phase ($\langle \bar{L} \rangle \simeq 0$),

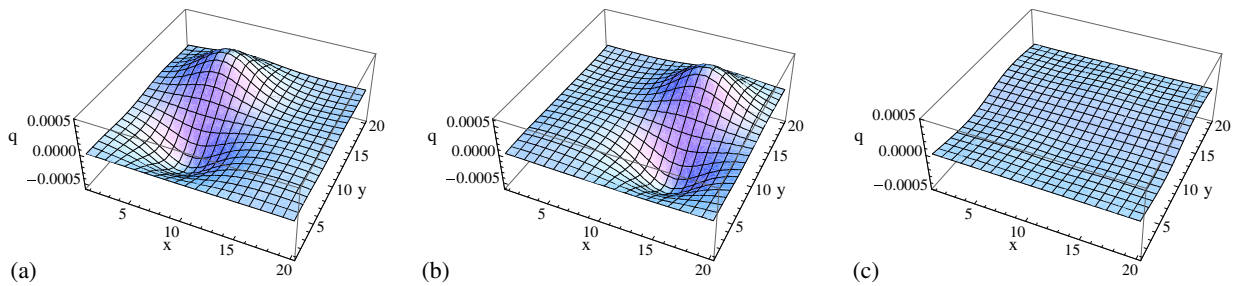

FIG. 6 (color online). For the light double-dyon–antidyon pair the reconstructed fermionic topological charge densities are shown in (a),(b),(c), corresponding to the three boundary conditions mentioned in the text.

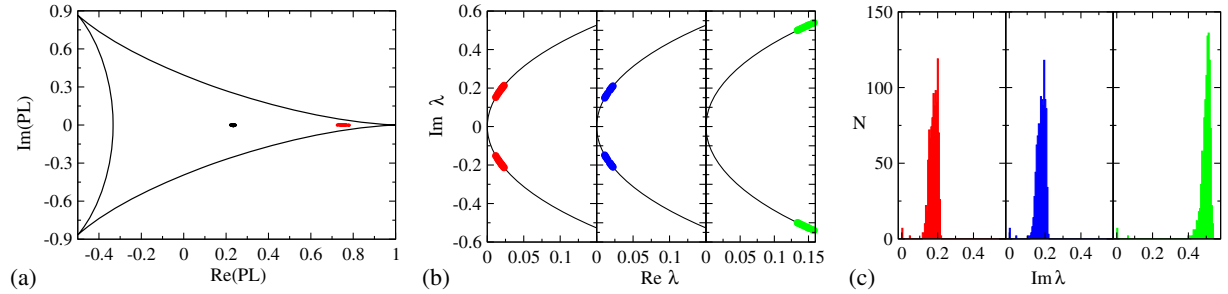

FIG. 7 (color online). (a) Scatter plot of the spatially averaged Polyakov loop $\bar{L}$ for 50 Monte Carlo generated configurations (shown in black symbols); the right group (of red points) refers to the values of $\bar{L}$ obtained after four steps of over-improved cooling. (b) Scatter plot of low-lying overlap eigenvalues for one of these configurations under the three boundary conditions and (c) corresponding distributions of the imaginary part of the overlap eigenvalues from all available configurations.

where we expect all the (anti)dyons occur with the same "mass" and statistical weight, respectively.)

That such a splitting may happen is supported by the following observation. The three eigenvalue spectra of the overlap operator obtained with the three boundary conditions [for a typical configuration see Fig. 7(b), for the whole ensemble compare with Fig. 7(c)] look different. The third boundary condition, which is the physical one in QCD with fermions, provides a much larger gap than the others. Thus, the spectra qualitatively resemble those observed for the light double-dyon–antidyon pair (first- and second-type dyons) as shown in Fig. 4. Therefore, we believe that light dyon-antidyon pairs (involving dyons of the two light species) form the bulk of configurations in the deconfinement phase and present further evidence below. Concerning the topological charge density, we have applied the same cluster analysis as in our previous paper [41] with a variable lower cutoff $q_{\rm cut} > 0$ to analyze the density functions of Eq. (21) for thermal configurations describing the deconfined phase. Let us repeat here the idea of the cluster algorithm.

In a first step–for each of the three fermionic boundary conditions Eq. (20)–the algorithm identifies the points forming the interior of all clusters (the so-called "topological cluster matter") defined by the condition $|q(x)| > q_{\rm cut}$. The crucial second step is to enquire the connectedness between the lattice points in order to form individual clusters out of this "cluster matter." Neighboring points with $|q(x)|$ above threshold and sharing the same sign of the topological charge density are defined to belong to the same cluster. The cutoff $q_{\rm cut}$ has been chosen such as to resolve the given continuous distribution $q(x)$ into a maximal number of internally connected, while mutually separated clusters. The cutoff value has been independently adapted for each configuration. As a result in the average the linear cluster size turns out approximately $3.2a \simeq 0.35$ fm.

We cannot exclude that this procedure might overestimate the number of separately counted clusters by inclusion of too small objects with too low density. But in any case, it allows us to discover extended objects that eventually can be qualified as (anti)dyons in the deconfined phase. There are two conditions to make this interpretation in each case more likely: the local correlation with timelike Abelian monopoles in MAG and the occurrence of nearly coinciding eigenvalues of the local holonomy in the centers of all clusters.

Thus, we have to inquire several criteria in order to enforce the evidence for the dyonic nature of these clusters in the deconfined phase, in the sense of being KvBLL caloron constituents. In our previous work [41] we have concentrated on the profile of the local Polyakov loop inside them, which points towards the relative closeness of two (or three) eigenvalues of the holonomy. Here additionally we use MAG monopoles as another feature characterizing dyons. We have seen this in the artificial examples of dyon-antidyon pairs considered in Section IV.

The removal of entropic monopole fluctuations (as result of over-improved cooling as mentioned above) renders all monopole loops static in temporal direction. Moreover, it maximizes the number of timelike monopole currents contained in topological clusters compared to the number of timelike monopole currents present in the whole lattice.

This latter criterion has been decisive to determine the actual number of sweeps of over-improved cooling (four). At this cooling stage the average action for the given volume turned out equal to $S = 61.2(2)S_{\rm inst}$. The (non-integer) gluonic topological charge $Q_{\rm glue}$ according to Eq. (11) for each configuration was found to be equal to the (integer) fermionic topological charge $Q_{\rm over}$ [given by the index of the overlap operator Eq. (16)] within 10% accuracy. In our ensemble of 50 configurations, we found 43 configurations with $Q_{\rm over} = 0$ and 7 configurations with $|Q_{\rm over}| = 1$, which leads for our temperature $T = 1.5T_d$ and lattice volume to a rough estimate of the (suppressed) topological susceptibility $\chi_t = \langle Q^2_{\rm over}\rangle/V \simeq (82\ {\rm MeV})^4$.

The three-dimensional projection of points belonging to topological clusters and the location of the static monopole loops after four sweeps of over-improved cooling steps are shown on Fig. 8 for a typical configuration.

All the data on the correlations between topological charge density and the MAG monopoles are presented in

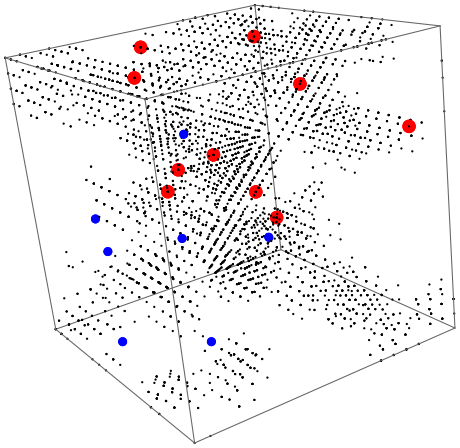

FIG. 8 (color online). The three-dimensional projection of points belonging to topological clusters (black small points) and the location of static timelike monopole loops after moderate over-improved cooling inside clusters (larger red spheres) and outside clusters (small blue spheres) are shown for one typical Monte Carlo generated gauge field configuration.

Table I where the corresponding data for cooled and original thermal configurations are shown for comparison. Also the data obtained with only ten of the lowest overlap modes used for determining the topological charge density are shown for comparison. Let us note that the MAG Gribov copy effects measured by the difference between results obtained with one and with ten gauge copies amounts to about 10% for equilibrium configurations. For cooled configurations the results do not differ within error bars. In the following we will discuss results obtained after cooling.

Our main results on the correlation of low-lying modes of the overlap Dirac operator (as represented by the clusters of fermionic topological charge) with the Abelian monopoles of MAG are as follows. Topological clusters occupy about 16.8% of the lattice volume, whereas topological clusters with static MAG monopoles cover only 9.7% of the lattice volume, but they contain about 35% of MAG monopoles. Inside topological clusters with MAG monopoles the latter are about 5 times more dense than outside these clusters. These numbers become even more pronounced if one counts not just the timelike monopole currents (dual links) in topological clusters but the numbers of thermal monopoles piercing topological clusters. Then around 50% of thermal monopoles are piercing topological clusters.

We expect that the topological clusters detected with antiperiodic boundary conditions (in our case with a real-valued average Polyakov loop) can be viewed as related to heavy dyons which in the deconfinement phase should become statistically suppressed because of their higher action in comparison with the other constituents of a caloron at a holonomy which is not maximally nontrivial. We can estimate this suppression quantitatively by measuring the abundance of MAG monopoles in topological clusters of the third type compared to those in topological clusters of the first or second type. We found after cooling and with twenty low-lying modes the proportion

TABLE I. Results of the cluster analysis using low-lying overlap operator modes with three kinds of boundary conditions, according to Eq. (20). All numbers indicate averages per configuration. The pure statistical errors are given in parentheses. We denote with $V_{\rm cl}$ the volume fraction occupied by all topological clusters, $V_{\rm cl\,mon}$ is the volume fraction occupied by clusters containing timelike magnetic monopoles, $N_{\rm cl}$ is the number of all clusters per configuration, $N_{\rm cl\,mon}$ is the number of clusters containing timelike magnetic monopoles, $N_{\rm mon}$ is the overall number of dual timelike links carrying monopole currents, $N_{\rm mon\,cl}$ is the number of dual timelike links with monopole currents found inside topological clusters, $N_{\rm loop}$ is the overall number of thermal monopoles, and $N_{\rm loop\,cl}$ is the number of timelike magnetic current loops piercing topological clusters. The effect of Gribov copies (see the text) on $N_{\rm mon}$ and $N_{\rm loop}$ for cooled and original configurations is indicated in the last lines of the upper two subtables by "../..".

Type of clusters	$V_{\rm cl}$	$V_{\rm cl\,mon}$	$N_{\rm cl}$	$N_{\rm cl\,mon}$	$N_{\rm mon}$	$N_{\rm mon\,cl}$	$N_{\rm loop}$	$N_{\rm loop\,cl}$
Clusters obtained with 20 lowest overlap modes, monopoles after cooling								
3rd type (heavy) clusters	4.3(3)%	1.1(2)%	20(1)	1.3(1)	⋯	3.6(5)	⋯	1.4(2)
1st type (light) clusters	8.5(6)%	5.4(6)%	25(1)	3.7(2)	⋯	14(1)	⋯	4.7(3)
2nd type (light) clusters	8.0(7)%	4.7(7)%	25(1)	3.4(2)	⋯	12(1)	⋯	4.3(3)
All clusters in total	16.8(7)%	9.7(7)%	70(1)	8.4(4)	60(2)/64(2)	21(1)	15(1)/16(1)	7.2(3)
Clusters obtained with 20 lowest overlap modes, monopoles before cooling								
3rd type (heavy) clusters	4.3(3)%	2.2(2)%	20(1)	4.3(3)	⋯	12(1)	⋯	4.4(3)
1st type (light) clusters	8.5(6)%	7.1(6)%	25(1)	7.2(3)	⋯	32(2)	⋯	11.8(7)
2nd type (light) clusters	8.0(7)%	6.5(6)%	25(1)	7.0(3)	⋯	29(2)	⋯	10.7(7)
All clusters in total	16.8(7)%	13.3(7)%	70(1)	18.5(6)	188(3)/210(4)	55(2)	32(1)/35(1)	18(1)
Clusters obtained with only 10 lowest overlap modes, monopoles after cooling								
3rd type (heavy) clusters	4.4(4)%	1.3(2)%	13(1)	1.3(1)	⋯	3.6(4)	⋯	1.4(1)
1st type (light) clusters	8(1)%	6(1)%	19(1)	3.0(2)	⋯	12(1)	⋯	4.2(3)
2nd type (light) clusters	10(1)%	8(1)%	18(1)	2.7(2)	⋯	12(1)	⋯	4.1(3)
All clusters in total	18(1)%	13(1)%	50(1)	7.0(3)	60(2)	21(1)	15(1)	6.9(3)

14:12:3.6 (see the upper subtable). Thus, the heavier caloron constituent clusters are really suppressed.

The following observations are also of interest. The average size of clusters with magnetic monopoles is about four times larger than the average size of clusters without magnetic monopoles, while their number is approximately an order of magnitude smaller. Clusters of third type (heavy dyons) are pierced just by one thermal (static) monopole world line. In the average, only 2.5 timelike currents of monopole loops (out of 4 belonging to a thermal monopole after cooling) are running inside these clusters.

In the case of topological clusters of first and second types (light dyon candidates) in the average three timelike currents of monopole loops (out of four belonging to a thermal monopole) are running inside these clusters. Moreover, approximately 30% of these clusters are pierced even by two monopole loops. In order to understand this observation one should take into account that clusters of the two light types occupy a volume approximately twice as large as that of clusters of the third type (identified as heavy dyons) and therefore, might overlap in space-time. Unfortunately, to distinguish the monopoles (to make the intersections one-to-one) is not a gauge-invariant concept.

Although the pattern of Polyakov loops becomes highly modified by cooling in the deconfined phase, it is possible to point out a correlation between the Polyakov loop on one side and monopoles, respective clusters of topological charge on the other.

First, let us compare the distributions of the minimal distance between eigenvalues of the local holonomies for all lattice sites and for sites carrying thermal monopoles. From analytical caloron solutions and from our artificial semianalytic configurations (see Figs. 2(c) and 5(c)) we know that in the center of a topological dyon cluster with a magnetic monopole the local holonomy has at least two identical eigenvalues. This means that the local Polyakov loop takes a value on one of the three sides of the Polyakov triangle (see the Appendix in Ref. [41]).

We quantify the closeness of a Polyakov loop value to the boundary of this triangle by the minimal distance $\min\{m_1(\vec{x}), m_2(\vec{x}), m_3(\vec{x})\}$, where the $m_i(\vec{x})$ are defined as the differences between the three eigenvalues $\mu_i(\vec{x})$ of the local holonomy according to Eqs. (4) and (5),

$$m_i(\vec{x}) = |\mu_{i+1}(\vec{x}) - \mu_i(\vec{x})|, \qquad i = 1, 2, 3,$$
$$\mu_4(\vec{x}) \equiv \mu_1(\vec{x}).$$

The two distributions with respect to the minimal distance are shown in Fig. 9 and tell that the local Polyakov loop at sites with thermal monopoles tend to be located closer to the boundary of the Polyakov triangle than for all lattice sites.

Second, we show the scatter plot of Polyakov loops measured (after cooling) in the centers of those clusters which are associated with magnetic monopoles. Since the clusters are labeled by one of the three boundary conditions for the fermionic modes (used to define the fermionic topological charge density), the scatter plot over the Polyakov triangle Fig. 10(a) shows the different regions of population. There is a tendency of the Polyakov loop in the centers of topological clusters of the two light kinds to populate two sides of the Polyakov triangle beginning from the trivial Polyakov loop $L \approx (1.0, 0.0)$. Compared with the results before cooling, the population has moved closer towards the trivial Polyakov loop and towards the periphery, thereby improving the (approximate) degeneracy of two eigenvalues of the local holonomy. From Fig. 10(a) we see also that clusters of the third type (which are heavy) are less abundant and distributed over most of the Polyakov triangle. Cooling has moved part of them towards the trivial Polyakov loop, too, but others are still differing strongly from trivial holonomy.

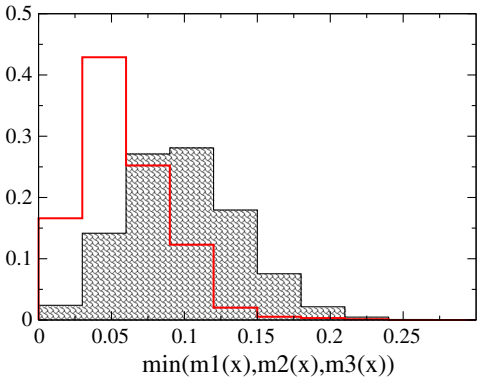

FIG. 9 (color online). For all lattice sites (shaded histogram) and for all cubes where thermal monopoles are located (open red histogram), the distributions with respect to the minimal distance $\min(m_1(\vec{x}), m_2(\vec{x}), m_3(\vec{x}))$ between the Polyakov loop and one of the boundaries of the Polyakov triangle are shown. In the case of a monopole the minimum is taken also among the eight corners of the three-dimensional cube containing that monopole.

Finally, if one extends the scatter plots by a third dimension representing the maximal absolute value of topological charge density of the corresponding clusters by spikes [see Fig. 10(b)] one observes the clusters of first and second type to have negligible topological charge, while the clusters of third type may carry noticeable topological charge (deserving the name heavy clusters). There is a tendency of heavy clusters to have a Polyakov loop opposite to the trivial one, $L \approx (1.0, 0.0)$.

In conclusion, the Polyakov loop characteristics of the "light plus heavy dyonic picture" for the clusters of topological charge in the deconfined phase are clearly visible after a slight cooling of the configurations.

VI. CONCLUSIONS

For $SU(3)$ gluodynamics we have discussed the signatures of dyonic topological excitations of thermal lattice gauge fields generated in the deconfinement phase. We

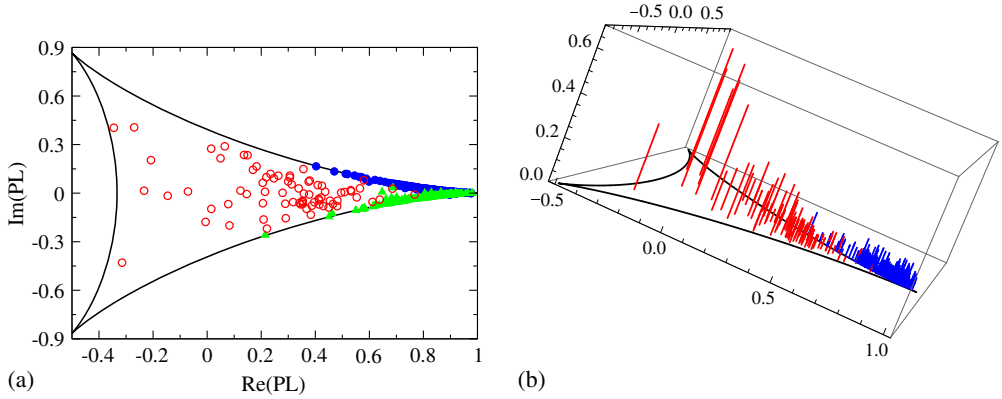

FIG. 10 (color online). (a) Scatter plots of Polyakov loop PL (after four steps of cooling) in clusters selected to contain monopoles. The clusters are separated according to the type of boundary condition for the overlap near-zero modes. For clusters of the first type, the Polyakov loop is shown by green triangles, for clusters of the second type, by blue filled circles, and for clusters of the third type, by red open circles. (b) The maximum of the topological charge density inside the respective cluster is additionally shown in respective color (for second and third type clusters only).

have chosen a temperature value $T = 1.5T_c$, i.e. well above the critical one. Under the assumption that (anti)dyon excitations become really relevant in the sense proposed by Diakonov and Petrov [26], we suppose them to be related to the constituents of KvBLL calorons [8–10] with an asymptotic holonomy determined by the average Polyakov loop (always taken in the real sector of the Polyakov triangle) which is then clearly different from zero (i.e. different from maximally nontrivial holonomy in the confinement phase). In this case the three monopole (dyon) constituents of KvBLL calorons are known to differ with respect to their masses or summed topological charges, the latter being directly related to the eigenvalues of the asymptotic holonomy. Then it is natural to conjecture that the heavy kind of dyons will be statistically suppressed compared with the light type. This means also that full KvBLL calorons should become rare excitations, too. It was our task to provide numerical evidence for this semiclassical-like dyon picture.

In order to find signatures of distinct light and heavy (anti)dyon pairs, we have first constructed classical model configurations from KvBLL (anti)caloron solutions with the help of an appropriate cut-and-paste procedure. For these configurations we checked the fermionic overlap eigenvalue spectrum and visualized them with several local observables:

(i) the gluonic topological density,
(ii) the fermionic topological density filtered with the low-lying modes of the overlap operator and determined with a set of three different timelike boundary conditions, such that each boundary condition extracts just one dyon type,
(iii) local values of the Polyakov loop as corresponding to the local holonomies for which the degeneracy of eigenvalues are pointing to the positions of the dyon constituents,
(iv) the Abelian monopole currents in the maximally Abelian gauge.

For the examples of a heavy dyon-antidyon pair and for a light double-dyon–antidyon pair, we produced a very clear pattern to be qualitatively compared with that of topological clusters of Monte Carlo generated quantum gauge fields.

Such topological clusters were then established by filtering with 20 low-lying modes of the overlap Dirac operator by employing the same three boundary conditions. Additionally, we subjected the lattice fields to a few (over-improved) cooling steps after which a similar pattern of clusters occurs with the gluonic topological charge distribution. With and without cooling, we looked for the behavior of the spatially averaged as well as the local distributions of the Polyakov loop (as well as its local holonomies) and searched for MAG monopole currents.

First of all—depending on the boundary conditions—we mostly found eigenvalue spectra similar to those produced by light dyon-antidyon pairs and rare cases telling about heavy dyon-antidyon pairs. Moreover, we found clear correlations of the topological clusters with thermal monopoles as well as with lattice sites, where the local holonomy has close-to-degenerate eigenvalues.

All this points to an interpretation in terms of mostly light—with only a dilute admixture of heavy—(anti)dyon excitations of the KvBLL type.

Moreover, our findings resemble very much what we found earlier in the $SU(2)$ case [38,42,44] where in the deconfinement phase the dominance of light dyon constituents was seen, too. F. Bruckmann [80], as well as more recently E. V. Shuryak and T. Sulejmanpasic in [33], came to a similar conclusion.

It remains to be seen how the situation will change in lattice QCD with dynamical fermions taken into account. We hope to come back to this question in the near future.

ACKNOWLEDGMENTS

The authors thank F. Bruckmann, E. V. Shuryak and V. Petrov for very useful comments. B. V. M. appreciates the support of Humboldt University Berlin where the main part of the work was finalized. E.-M. I. and M. M.-P. acknowledge financial support by the Heisenberg-Landau Program of the Bogolubov Laboratory of Theoretical Physics at JINR Dubna. V. G. B. has been supported by the Grant RFBR No. 13-02-01387a. This work was much influenced by Pierre van Baal and Dmitri Igorevich Diakonov, who both sadly passed away.

[1] P. H. Ginsparg and K. G. Wilson, Phys. Rev. D **25**, 2649 (1982).
[2] F. Niedermayer, Nucl. Phys. B, Proc. Suppl. **73**, 105 (1999).
[3] H. Neuberger, Phys. Lett. B **417**, 141 (1998).
[4] H. Neuberger, Phys. Lett. B **427**, 353 (1998).
[5] P. Hasenfratz, V. Laliena, and F. Niedermayer, Phys. Lett. B **427**, 125 (1998).
[6] T. Schäfer and E. V. Shuryak, Rev. Mod. Phys. **70**, 323 (1998).
[7] T. C. Kraan and P. van Baal, Phys. Lett. B **428**, 268 (1998).
[8] T. C. Kraan and P. van Baal, Phys. Lett. B **435**, 389 (1998).
[9] T. C. Kraan and P. van Baal, Nucl. Phys. **B533**, 627 (1998).
[10] K.-M. Lee and C.-H. Lu, Phys. Rev. D **58**, 025011 (1998).
[11] M. C. Chu, J. M. Grandy, S. Huang, and J. W. Negele, Phys. Rev. D **49**, 6039 (1994).
[12] J. W. Negele, arXiv:hep-lat/9804017.
[13] R. Brower, D. Chen, J. W. Negele, K. Orginos, and C.-I. Tan, Nucl. Phys. B, Proc. Suppl. **73**, 557 (1999).
[14] J. W. Negele, Nucl. Phys. B, Proc. Suppl. **73**, 92 (1999).
[15] E.-M. Ilgenfritz, B. V. Martemyanov, M. Müller-Preussker, S. Shcheredin, and A. I. Veselov, Phys. Rev. D **66**, 074503 (2002).
[16] F. Bruckmann, D. Nogradi, and P. van Baal, Nucl. Phys. **B698**, 233 (2004).
[17] M. Fukushima, A. Tanaka, S. Sasaki, H. Suganuma, H. Toki, and D. Diakonov, Nucl. Phys. B, Proc. Suppl. **53**, 494 (1997).
[18] M. Fukushima, S. Sasaki, H. Suganuma, A. Tanaka, H. Toki, and D. Diakonov, Phys. Lett. B **399**, 141 (1997).
[19] D. Diakonov, Prog. Part. Nucl. Phys. **51**, 173 (2003).
[20] D. Diakonov, N. Gromov, V. Petrov, and S. Slizovskiy, Phys. Rev. D **70**, 036003 (2004).
[21] T. C. Kraan, Commun. Math. Phys. **212**, 503 (2000).
[22] D. Diakonov and N. Gromov, Phys. Rev. D **72**, 025003 (2005).
[23] P. Gerhold, E.-M. Ilgenfritz, and M. Müller-Preussker, Nucl. Phys. **B760**, 1 (2007).
[24] B. J. Harrington and H. K. Shepard, Phys. Rev. D **17**, 2122 (1978).
[25] A. M. Polyakov, Nucl. Phys. **B120**, 429 (1977).
[26] D. Diakonov and V. Y. Petrov, Phys. Rev. D **76**, 056001 (2007).
[27] F. Bruckmann, S. Dinter, E.-M. Ilgenfritz, M. Müller-Preussker, and M. Wagner, Phys. Rev. D **79**, 116007 (2009).
[28] F. Bruckmann, S. Dinter, E.-M. Ilgenfritz, B. Maier, M. Müller-Preussker, and M. Wagner, Phys. Rev. D **85**, 034502 (2012).
[29] V. A. Fateev, I. V. Frolov, and A. S. Schwarz, Nucl. Phys. **B154**, 1 (1979).
[30] B. Berg and M. Lüscher, Commun. Math. Phys. **69**, 57 (1979).
[31] E. V. Shuryak and T. Sulejmanpasic, Phys. Rev. D **86**, 036001 (2012).
[32] P. Faccioli and E. V. Shuryak, Phys. Rev. D **87**, 074009 (2013).
[33] E. V. Shuryak and T. Sulejmanpasic, Phys. Lett. B **726**, 257 (2013).
[34] C. Gattringer, E.-M. Ilgenfritz, B. V. Martemyanov, M. Müller-Preussker, D. Peschka, R. Pullirsch, S. Schaefer, and A. Schäfer, Nucl. Phys. B, Proc. Suppl. **129–130**, 653 (2004).
[35] E.-M. Ilgenfritz, B. V. Martemyanov, M. Müller-Preussker, and A. I. Veselov, Phys. Rev. D **69**, 114505 (2004).
[36] E.-M. Ilgenfritz, B. V. Martemyanov, M. Müller-Preussker, and A. I. Veselov, Phys. Rev. D **71**, 034505 (2005).
[37] E.-M. Ilgenfritz, M. Müller-Preussker, and D. Peschka, Phys. Rev. D **71**, 116003 (2005).
[38] E.-M. Ilgenfritz, B. V. Martemyanov, M. Müller-Preussker, and A. I. Veselov, Phys. Rev. D **73**, 094509 (2006).
[39] F. Bruckmann, E.-M. Ilgenfritz, B. V. Martemyanov, M. Müller-Preussker, D. Nogradi, D. Peschka, and P. van Baal, Nucl. Phys. B, Proc. Suppl. **140**, 635 (2005).
[40] F. Bruckmann, E.-M. Ilgenfritz, B. V. Martemyanov, and P. van Baal, Phys. Rev. D **70**, 105013 (2004).
[41] E.-M. Ilgenfritz, B. V. Martemyanov, and M. Müller-Preussker, Phys. Rev. D **89**, 054503 (2014).
[42] V. G. Bornyakov, E.-M. Ilgenfritz, B. V. Martemyanov, S. M. Morozov, M. Müller-Preussker, and A. I. Veselov, Phys. Rev. D **76**, 054505 (2007).
[43] V. G. Bornyakov, E. V. Luschevskaya, S. M. Morozov, M. I. Polikarpov, E.-M. Ilgenfritz, and M. Müller-Preussker, Phys. Rev. D **79**, 054505 (2009).
[44] V. G. Bornyakov, E.-M. Ilgenfritz, B. V. Martemyanov, and M. Müller-Preussker, Phys. Rev. D **79**, 034506 (2009).
[45] M. N. Chernodub, T. C. Kraan, and P. van Baal, arXiv:hep-lat/9907001.
[46] D. J. Gross, R. D. Pisarski, and L. G. Yaffe, Rev. Mod. Phys. **53**, 43 (1981).

[47] M. García Pérez, A. González-Arroyo, J. R. Snippe, and P. van Baal, Nucl. Phys. **B413**, 535 (1994).
[48] V. G. Bornyakov, E.-M. Ilgenfritz, B. V. Martemyanov, V. K. Mitrjushkin, and M. Müller-Preussker, Phys. Rev. D **87**, 114508 (2013).
[49] V. G. Bornyakov, V. K. Mitrjushkin, and M. Müller-Preussker, Phys. Lett. B **284**, 99 (1992).
[50] M. N. Chernodub, A. D'Alessandro, M. D'Elia, and V. I. Zakharov, arXiv:0909.5441.
[51] M. N. Chernodub and V. I. Zakharov, Phys. Rev. Lett. **98**, 082002 (2007).
[52] V. G. Bornyakov, A. G. Kononenko, and V. K. Mitrjushkin, *Proc. Sci.*, LATTICE (2013) 358.
[53] M. Lüscher and P. Weisz, Commun. Math. Phys. **97**, 59 (1985).
[54] E.-M. Ilgenfritz, K. Koller, Y. Koma, G. Schierholz, T. Streuer, and V. Weinberg, Phys. Rev. D **76**, 034506 (2007).
[55] C. Gattringer, R. Hoffmann, and S. Schaefer, Phys. Rev. D **65**, 094503 (2002).
[56] C. Gattringer, M. Göckeler, P. Rakow, S. Schaefer, and A. Schäfer, Nucl. Phys. **B618**, 205 (2001).
[57] M. Lüscher and P. Weisz, Phys. Lett. **158B**, 250 (1985).
[58] J. R. Snippe, Nucl. Phys. **B498**, 347 (1997).
[59] G. P. Lepage and P. B. Mackenzie, Phys. Rev. D **48**, 2250 (1993).
[60] G. Endrodi, C. Gattringer, and H.-P. Schadler, Phys. Rev. D **89**, 054509 (2014).
[61] S. O. Bilson-Thompson, D. B. Leinweber, and A. G. Williams, Ann. Phys. (Amsterdam) **304**, 1 (2003).
[62] C. Bonati and M. D'Elia, Phys. Rev. D **89**, 105005 (2014).
[63] M. Lüscher, Commun. Math. Phys. **293**, 899 (2010).
[64] M. Lüscher, J. High Energy Phys. 08 (2010) 071.
[65] M. Lüscher and P. Weisz, J. High Energy Phys. 02 (2011) 051.
[66] E. Bilgici, F. Bruckmann, J. Danzer, C. Gattringer, C. Hagen, E.-M. Ilgenfritz, and A. Maas, Few Body Syst. **47**, 125 (2010).
[67] F. Bruckmann, C. Gattringer, E.-M. Ilgenfritz, M. Müller-Preussker, A. Schäfer, and S. Solbrig, Eur. Phys. J. A **33**, 333 (2007).
[68] E.-M. Ilgenfritz, D. Leinweber, P. Moran, K. Koller, G. Schierholz, and V. Weinberg, Phys. Rev. D **77**, 074502 (2008).
[69] F. Bruckmann, F. Gruber, C. Lang, M. Limmer, T. Maurer, A. Schäfer, and S. Solbrig, *Proc. Sci.*, CONFINEMENT (2008) 045.
[70] A. S. Kronfeld, G. Schierholz, and U. Wiese, Nucl. Phys. **B293**, 461 (1987).
[71] F. Brandstaeter, U. J. Wiese, and G. Schierholz, Phys. Lett. B **272**, 319 (1991).
[72] W. W. Tucker and J. D. Stack, Nucl. Phys. B, Proc. Suppl. **106–107**, 643 (2002).
[73] C. Bonati and M. D'Elia, Nucl. Phys. **B877**, 233 (2013).
[74] G. S. Bali, V. G. Bornyakov, M. Müller-Preussker, and K. Schilling, Phys. Rev. D **54**, 2863 (1996).
[75] V. G. Bornyakov, G. Schierholz, and T. Streuer, Nucl. Phys. B, Proc. Suppl. **106–107**, 676 (2002).
[76] V. G. Bornyakov *et al.* (DIK Collaboration), Phys. Rev. D **70**, 074511 (2004).
[77] V. G. Bornyakov *et al.* (DIK Collaboration), Phys. Rev. D **71**, 114504 (2005).
[78] P. Van Baal, Nucl. Phys. B, Proc. Suppl. **108**, 3 (2002).
[79] R. Larsen and E. V. Shuryak, arXiv:1408.6563.
[80] F. Bruckmann, *Proc. Sci.*, CONFINEMENT (2008) 179.